Frequency Response Data-based Resonant Filter Design considering Phase Stabilization and Stroke Limitation applied to Dual-Stage Actuator Hard Disk Drives

Masahiro Mae * **Wataru Ohnishi** * **Hiroshi Fujimoto** *

* *Department of Electrical Engineering and Information Systems, Graduate School of Engineering, The University of Tokyo, Japan.*
(e-mail: mmae@ieee.org)

Abstract: Disturbance rejection of a Hard Disk Drive (HDD) enables a large amount of data storage in a recent information society. The aim is to design a feedback controller which rejects disturbances at multiple frequencies in HDDs. The disturbance rejection is achieved using resonant filters which have a large peak at disturbance frequencies. The developed approach enables the convex optimization of resonant filters with phase stabilization and stroke limitation using frequency response data of a controlled system. The disturbance rejection performance of the optimized resonant filters is validated in a dual-stage actuator HDD benchmark problem.

Keywords: disturbance rejection, positioning control, data-based design, convex optimization, frequency response, hard disk drive

1. INTRODUCTION

Increasing demand for storage capacity of data servers in a recent information society leads to the importance of the track-following performance in a Hard Disk Drive (HDD) (Atsumi, 2016). To improve the track-following performance, the feedback controller should be designed to reject disturbances in HDDs.

Model-based approaches are traditionally developed such as using adaptive control (Ohno and Hara, 2006; Pérez-Arancibia et al., 2010; Shahsavari et al., 2015; Sun et al., 2017), resonant filter (Atsumi et al., 2007), repetitive control (Fujimoto, 2009; Chen and Tomizuka, 2014), Youla–Kucera parameterization (Chen and Tomizuka, 2016), disturbance observer (Zheng et al., 2017), and coupling controller (Yabui et al., 2020). They basically need a modeling process of a controlled system that makes it difficult to consider model variations of mass-produced HDDs. These approaches also need a heuristic tuning process. Data-based approaches are also developed to recover disadvantages of model-based approaches such as using H_∞ and H_2 robust control (Bashash and Shariat, 2019; Potu Surya Prakash and Horowitz, 2022). These approaches only consider the gain stabilization and it can result in a conservative controller design. Hardware constraints such as maximum strokes also should be considered for actual implementation.

Although important contributions have been made to design feedback controllers for disturbance rejection in HDDs, phase stabilization and stroke limitation are not considered in the optimization of feedback controllers. In this paper, the developed approach enables the structured multiple resonant filter design considering phase stabilization and stroke limitation.

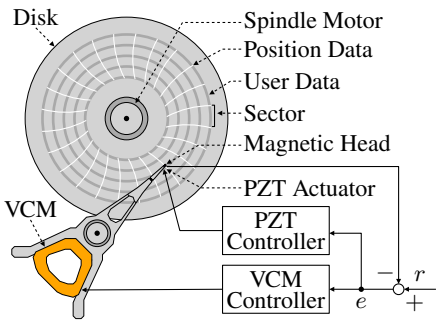

Fig. 1. Hard disk drive with a dual-stage actuator.

The main contributions of this paper are as follows.

(1) Resonant filters for a dual-input single-output system are designed by iterative convex optimization.
(2) Model variations of HDDs are directly dealt with multiple sets of frequency response data.
(3) Phase stabilization and stroke limitation are considered in optimization calculation.

2. PROBLEM FORMULATION

Fig. 1 illustrates the basic schematic of a dual-stage actuator HDD. This HDD consists of a Voice Coil Motor (VCM) and a PieZoelecTric (PZT) actuator. The objective of this benchmark problem is to minimize the tracking error of the magnetic head (Atsumi, 2022). The track-following performance is evaluated in $3\sigma(y_c)$ the worst case of three times of standard deviation value of the continuous-time magnetic head position in steady state response for 1 s. The track pitch is $T_p = 52.7\,\mathrm{nm}$ and sampling time is $T_s = 1/(7200/60)/420 \simeq 1.9841 \times 10^{-6}\,\mathrm{s}$.

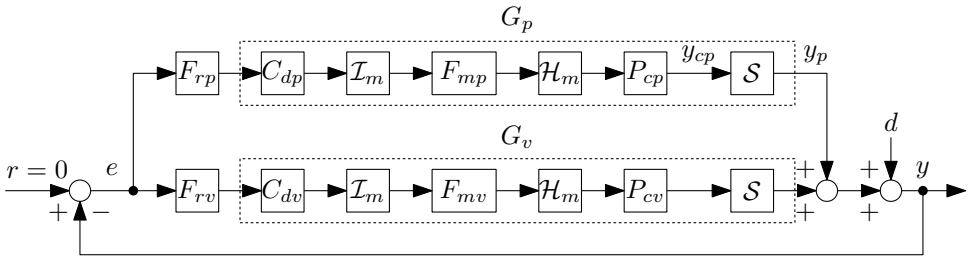

Fig. 2. Block diagram of a hard disk drive with a dual-stage actuator.

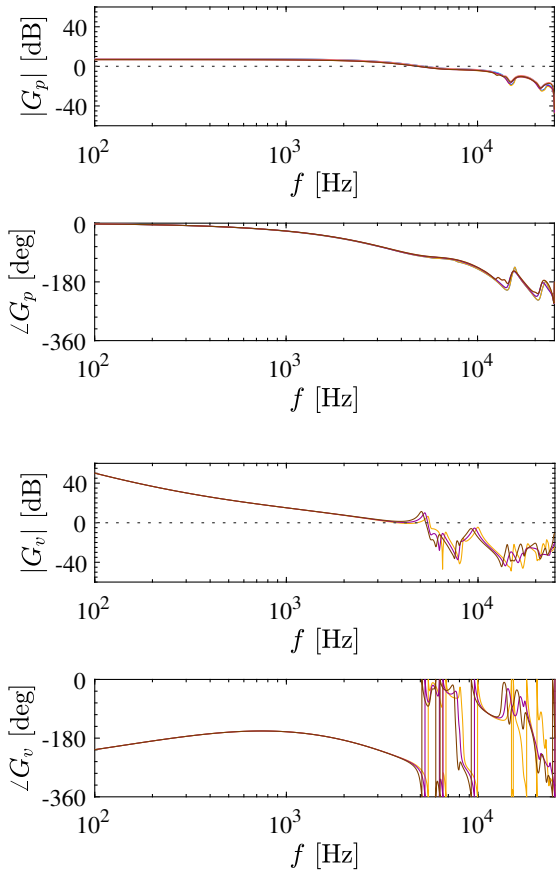

Fig. 3. Frequency responses of given open-loop systems. Top: PZT actuator G_p. Bottom: VCM G_v.

Because of the hardware constraints, the output stroke of the PZT actuator must be smaller than 50 nm.

Fig. 2 shows the block diagram of the dual-stage actuator HDD with continuous-time control systems P_c, discrete-time feedback controllers C_d, discrete-time multirate filters F_m. The subscripts p and v denote a PZT actuator and VCM, respectively. The continuous-time control system has 9 cases of model variations and the subscript $k_c = 1, \ldots, 9$ denotes the index of the 9 cases. $m \in \mathbb{N}$ is the number of multirate. $\mathcal{I}_m$ is interpolator for m times upsampling. $\mathcal{H}_m$ is multirate zero-order-hold in m times upsample. $\mathcal{S}$ is sampler.

The frequency response data of the given open-loop controlled systems G_p and G_v in Fig. 2 that consists of the controlled systems and pre-designed feedback controllers (Atsumi, 2022) is shown in Fig. 3. In this benchmark problem, the external disturbances consist of repeatable run-out d_{RRO}, rotational vibration d_f, and fan-induced vibration d_p. These three disturbances can be combined to one output disturbance d equivalently that is given by

$$d_{k_c}(\mathrm{j}\omega_{k_f}) = P_{cv,k_c}(\mathrm{j}\omega_{k_f})d_f(\mathrm{j}\omega_{k_f}) + d_p(\mathrm{j}\omega_{k_f}) - d_{\mathrm{RRO}}(\mathrm{j}\omega_{k_f}). \quad (1)$$

The amplitude spectrum of the output disturbance d in 9 cases is shown in Fig. 4.

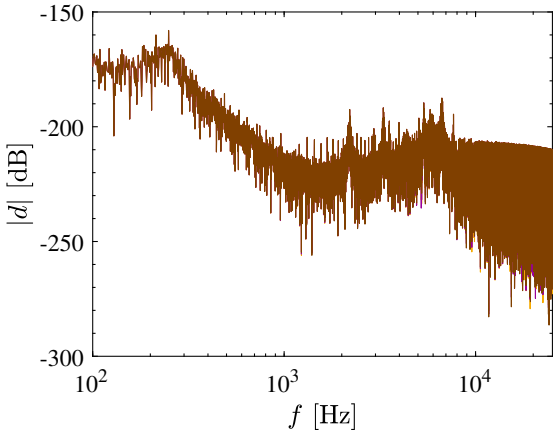

Fig. 4. Amplitude spectrum of output disturbances.

In this paper, the reference signal is $r = 0$ in all time and the objective is designing the resonant filters F_{rp} and F_{rv} for each actuator in addition to given open-loop controlled system G_p and G_v to minimize the worst case of track-following error against to the output disturbance d.

3. CONVEX OPTIMIZATION OF MULTIPLE RESONANT FILTERS UNDER CONSTRAINTS

In this section, the optimization method of multiple resonant filters for a dual-stage actuator HDD is formulated. The structure of the designed resonant filters is presented. The optimization problem that directly uses frequency response data is formulated with conditions of robust stability, robust performance, and hardware constraints. The optimization problem is solved by iterative convex optimization with sequential linearization.

3.1 Structure of designed resonant filters

To improve the track-following performance, disturbances can be rejected by the resonant filters (Atsumi et al., 2007) that have the same resonance frequency as the disturbance frequencies because of the internal model principle. In this paper, multiple resonant filters are designed in disturbance frequencies to improve the track-following performance.

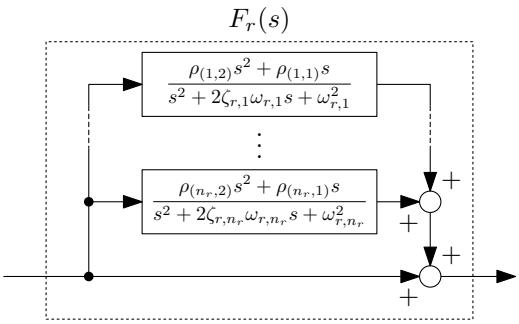

Fig. 5. Block diagram of resonant filters.

The block diagram of the designed resonant filters with multiple resonance frequencies is shown in Fig. 5. The resonant filter in each actuator is defined as

$$
\begin{aligned}
&F_{r,k_u}(\mathrm{j}\omega_{k_f},\boldsymbol{\rho}_{k_u}) \\
&= 1+\sum_{k_r=1}^{n_r}\frac{\rho_{k_u,(k_r,2)}(\mathrm{j}\omega_{k_f})^2+\rho_{k_u,(k_r,1)}(\mathrm{j}\omega_{k_f})}{(\mathrm{j}\omega_{k_f})^2+2\zeta_{r,k_r}\omega_{r,k_r}(\mathrm{j}\omega_{k_f})+\omega_{r,k_r}^2} \\
&= \begin{bmatrix} 1 \\ \rho_{k_u,(1,1)} \\ \rho_{k_u,(1,2)} \\ \vdots \\ \rho_{k_u,(n_r,1)} \\ \rho_{k_u,(n_r,2)} \end{bmatrix}^{\mathsf{T}} \begin{bmatrix} 1 \\ \frac{(\mathrm{j}\omega_{k_f})}{(\mathrm{j}\omega_{k_f})^2+2\zeta_{r,1}\omega_{r,1}(\mathrm{j}\omega_{k_f})+\omega_{r,1}^2} \\ \frac{(\mathrm{j}\omega_{k_f})^2}{(\mathrm{j}\omega_{k_f})^2+2\zeta_{r,1}\omega_{r,1}(\mathrm{j}\omega_{k_f})+\omega_{r,1}^2} \\ \vdots \\ \frac{(\mathrm{j}\omega_{k_f})}{(\mathrm{j}\omega_{k_f})^2+2\zeta_{r,n_r}\omega_{r,n_r}(\mathrm{j}\omega_{k_f})+\omega_{r,n_r}^2} \\ \frac{(\mathrm{j}\omega_{k_f})^2}{(\mathrm{j}\omega_{k_f})^2+2\zeta_{r,n_r}\omega_{r,n_r}(\mathrm{j}\omega_{k_f})+\omega_{r,n_r}^2} \end{bmatrix} \\
&= \boldsymbol{\rho}_{k_u}^{\mathsf{T}}\boldsymbol{\phi}(\mathrm{j}\omega_{k_f}), \qquad (2)
\end{aligned}
$$

where the subscripts that correspond to each actuator is $k_u \in \{p, v\}$, the number of designed resonance frequency is $n_r \in \mathbb{N}$, the index of the resonance frequency is $k_r = 1, \ldots, n_r$, the tuning parameter is $\boldsymbol{\rho} = [\boldsymbol{\rho}_p, \boldsymbol{\rho}_v]$ that consists of $\boldsymbol{\rho}_{k_u} \in \mathbb{R}^{2n_r+1}$, the resonance angular frequency is ω_{r,k_r}, and the damping coefficient is ζ_{r,k_r}.

The designed resonant filter consists of the sum of the resonant modes and phase compensators that are defined as

$$F(s) = \frac{\kappa s^2 + \kappa\psi s}{s^2 + 2\zeta_r\omega_r s + \omega_r^2}. \qquad (3)$$

Fig. 6 shows the vector locus using a resonant filter and the coefficients κ and ψ represent the gain and phase of each resonant mode.

3.2 Optimization problem formulation

In this paper, robust stability, robust performance, and hardware constraints are considered in frequency response data. For robust performance, the resonant filters are optimized to minimize the worst case of the error amplitude spectrum. For hardware constraints, the stroke limitation of the PZT actuator is considered that the maximum amplitude spectrum of y_p is less than the maximum value with the given feedback controller. For robust stability, the vector locus with resonant filters must be on the same side against $(-1, \mathrm{j}0)$ and at the outside of the modulus

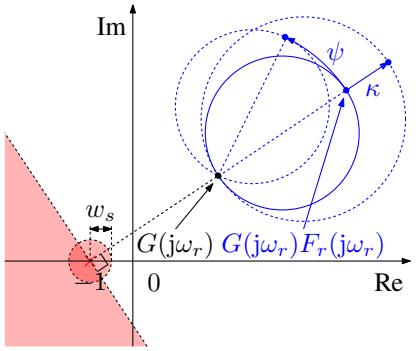

Fig. 6. Vector locus using a resonant filter with modulus margin and phase stabilization in Nyquist diagram.

margin. From these conditions, the optimization problem is formulated as follows.

$$\underset{\boldsymbol{\rho}}{\text{minimize}} \quad \max_{\forall k_c, \forall k_f} |e_{k_c}(\mathrm{j}\omega_{k_f})| \qquad (4a)$$

$$\text{subject to} \quad |y_{p,k_c}(\mathrm{j}\omega_{k_f})| \le y_{p,\max} \qquad (4b)$$

$$w_s(\mathrm{j}\omega_{k_f})|S_{k_c}(\mathrm{j}\omega_{k_f},\boldsymbol{\rho})| \le 1 \qquad (4c)$$

$$-\frac{\pi}{2} \le \angle\left(1+L_{k_c}(\mathrm{j}\omega_{k_f},\boldsymbol{\rho})\right) - \angle\left(1+G_{k_c}(\mathrm{j}\omega_{k_f})\right) \le \frac{\pi}{2}, \qquad (4d)$$

where w_s is the weighting of the sensitivity function and

$$G_{k_c}(\mathrm{j}\omega_r) = G_{p,k_c}(\mathrm{j}\omega_{k_f}) + G_{v,k_c}(\mathrm{j}\omega_{k_f}), \qquad (5)$$

$$L_{k_c}(\mathrm{j}\omega_{k_f},\boldsymbol{\rho}) = L_{p,k_c}(\mathrm{j}\omega_{k_f},\boldsymbol{\rho}_p) + L_{v,k_c}(\mathrm{j}\omega_{k_f},\boldsymbol{\rho}_v), \qquad (6)$$

$$L_{p,k_c}(\mathrm{j}\omega_{k_f},\boldsymbol{\rho}_p) = G_{p,k_c}(\mathrm{j}\omega_{k_f})F_{rp}(\mathrm{j}\omega_{k_f},\boldsymbol{\rho}_p), \qquad (7)$$

$$L_{v,k_c}(\mathrm{j}\omega_{k_f},\boldsymbol{\rho}_v) = G_{v,k_c}(\mathrm{j}\omega_{k_f})F_{rv}(\mathrm{j}\omega_{k_f},\boldsymbol{\rho}_v), \qquad (8)$$

$$S_{k_c}(\mathrm{j}\omega_{k_f},\boldsymbol{\rho}) = \frac{1}{1+L_{k_c}(\mathrm{j}\omega_{k_f},\boldsymbol{\rho})}. \qquad (9)$$

3.3 Convex optimization using sequential linearization

In (4a), the objective function can be equivalently given by

$$
\begin{aligned}
&\underset{\boldsymbol{\rho}}{\text{minimize}} \max_{\forall k_c, \forall k_f} |e_{k_c}(\mathrm{j}\omega_{k_f})| \Leftrightarrow \underset{\boldsymbol{\rho}}{\text{maximize}} \min_{\forall k_c, \forall k_f} \frac{1}{|e_{k_c}(\mathrm{j}\omega_{k_f})|} \\
&\Leftrightarrow \underset{\boldsymbol{\rho}}{\text{minimize}} -\left(\min_{\forall k_c, \forall k_f}\left|\frac{1}{d_{k_c}(\mathrm{j}\omega_{k_f})}\left(1+L_{k_c}(\mathrm{j}\omega_{k_f},\boldsymbol{\rho})\right)\right|\right), \qquad (10)
\end{aligned}
$$

where the error frequency response data is given by

$$e_{k_c}(\mathrm{j}\omega_{k_f}) = S_{k_c}(\mathrm{j}\omega_{k_f},\boldsymbol{\rho})d_{k_c}(\mathrm{j}\omega_{k_f}). \qquad (11)$$

In (4b), the amplitude spectrum of the output of the PZT actuator is evaluated as

$$|y_{p,k_c}(\mathrm{j}\omega_{k_f})| = \left|\frac{L_{p,k_c}(\mathrm{j}\omega_{k_f},\boldsymbol{\rho}_p)d_{k_c}(\mathrm{j}\omega_{k_f})}{1+L_{k_c}(\mathrm{j}\omega_{k_f},\boldsymbol{\rho})}\right|, \qquad (12)$$

and the maximum value with the given feedback controller is given by

$$y_{p,\max} = \max_{\forall k_c, \forall k_f}\left|\frac{G_{p,k_c}(\mathrm{j}\omega_{k_f})d_{k_c}(\mathrm{j}\omega_{k_f})}{1+G_{k_c}(\mathrm{j}\omega_{k_f})}\right|. \qquad (13)$$

In (4d), the angle of the vector locus is evaluated by atan2 function using the real and imaginary part of the vector locus. From these analyses, the optimization problem is given by (14).

The optimization problem (14) is nonlinear and non-convex. Using sequential linearization, the optimization problem can be calculated by the iterative convex optimization and is given by (15).

$$\underset{\boldsymbol{\rho}}{\text{minimize}} \quad -\gamma \tag{14a}$$

$$\underset{\forall k_c, \forall k_f}{\text{subject to}} \quad \gamma - \left| \frac{1}{d_{k_c}(\mathrm{j}\omega_{k_f})} \left(1 + L_{k_c}(\mathrm{j}\omega_{k_f}, \boldsymbol{\rho})\right) \right| \leq 0 \tag{14b}$$

$$\frac{|d_{k_c}(\mathrm{j}\omega_{k_f})|}{y_{p,\max}} \left| L_{p,k_c}(\mathrm{j}\omega_{k_f}, \boldsymbol{\rho}_p) \right| - \left| 1 + L_{k_c}(\mathrm{j}\omega_{k_f}, \boldsymbol{\rho}) \right| \leq 0 \tag{14c}$$

$$w_s(\mathrm{j}\omega_{k_f}) - \left| 1 + L_{k_c}(\mathrm{j}\omega_{k_f}, \boldsymbol{\rho}) \right| \leq 0 \tag{14d}$$

$$\mp \operatorname{atan2}\left(\frac{\operatorname{Im}(1 + L_{k_c}(\mathrm{j}\omega_{k_f}, \boldsymbol{\rho}))}{\operatorname{Re}(1 + L_{k_c}(\mathrm{j}\omega_{k_f}, \boldsymbol{\rho}))} \right) \pm \operatorname{atan2}\left(\frac{\operatorname{Im}(1 + G_{k_c}(\mathrm{j}\omega_{k_f}))}{\operatorname{Re}(1 + G_{k_c}(\mathrm{j}\omega_{k_f}))} \right) - \frac{\pi}{2} \leq 0 \text{ when } \pm \operatorname{Re}(1 + G_{k_c}(\mathrm{j}\omega_{k_f})) \geq 0 \tag{14e}$$

$$\pm \operatorname{atan2}\left(\frac{\operatorname{Im}(1 + L_{k_c}(\mathrm{j}\omega_{k_f}, \boldsymbol{\rho}))}{\operatorname{Re}(1 + L_{k_c}(\mathrm{j}\omega_{k_f}, \boldsymbol{\rho}))} \right) \mp \operatorname{atan2}\left(\frac{\operatorname{Im}(1 + G_{k_c}(\mathrm{j}\omega_{k_f}))}{\operatorname{Re}(1 + G_{k_c}(\mathrm{j}\omega_{k_f}))} \right) - \frac{\pi}{2} \leq 0 \text{ when } \pm \operatorname{Re}(1 + G_{k_c}(\mathrm{j}\omega_{k_f})) \geq 0 \tag{14f}$$

$$\underset{\boldsymbol{\rho}_{k_i}}{\text{minimize}} \quad -\gamma \tag{15a}$$

$$\underset{\forall k_c, \forall k_f}{\text{subject to}} \quad \gamma - \operatorname{Re}\left(\frac{\left(\frac{1}{d_{k_c}(\mathrm{j}\omega_{k_f})}(1 + L_{k_c}(\mathrm{j}\omega_{k_f}, \boldsymbol{\rho}_{k_i - 1})) \right)^*}{\left| \frac{1}{d_{k_c}(\mathrm{j}\omega_{k_f})}(1 + L_{k_c}(\mathrm{j}\omega_{k_f}, \boldsymbol{\rho}_{k_i - 1})) \right|} \left(\frac{1}{d_{k_c}(\mathrm{j}\omega_{k_f})}(1 + L_{k_c}(\mathrm{j}\omega_{k_f}, \boldsymbol{\rho}_{k_i})) \right) \right) \leq 0 \tag{15b}$$

$$\frac{|d_{k_c}(\mathrm{j}\omega_{k_f})|}{y_{p,\max}} \operatorname{Re}\left(\frac{\left(L_{p,k_c}(\mathrm{j}\omega_{k_f}, \boldsymbol{\rho}_{p,k_i - 1})\right)^*}{\left|L_{p,k_c}(\mathrm{j}\omega_{k_f}, \boldsymbol{\rho}_{p,k_i - 1})\right|} \left(L_{p,k_c}(\mathrm{j}\omega_{k_f}, \boldsymbol{\rho}_{p,k_i})\right) \right) - \operatorname{Re}\left(\frac{\left(1 + L_{k_c}(\mathrm{j}\omega_{k_f}, \boldsymbol{\rho}_{k_i - 1})\right)^*}{\left|1 + L_{k_c}(\mathrm{j}\omega_{k_f}, \boldsymbol{\rho}_{k_i - 1})\right|} \left(1 + L_{k_c}(\mathrm{j}\omega_{k_f}, \boldsymbol{\rho}_{k_i})\right) \right) \leq 0 \tag{15c}$$

$$w_s(\mathrm{j}\omega_{k_f}) - \operatorname{Re}\left(\frac{\left(1 + L_{k_c}(\mathrm{j}\omega_{k_f}, \boldsymbol{\rho}_{k_i - 1})\right)^*}{\left|1 + L_{k_c}(\mathrm{j}\omega_{k_f}, \boldsymbol{\rho}_{k_i - 1})\right|} \left(1 + L_{k_c}(\mathrm{j}\omega_{k_f}, \boldsymbol{\rho}_{k_i})\right) \right) \leq 0 \tag{15d}$$

$$\mp \left(\operatorname{atan2}\left(\frac{\operatorname{Im}(1 + L_{k_c,k_i-1}(\mathrm{j}\omega_{k_f}, \boldsymbol{\rho}))}{\operatorname{Re}(1 + L_{k_c,k_i-1}(\mathrm{j}\omega_{k_f}, \boldsymbol{\rho}))} \right) + \frac{\operatorname{Re}(1 + L_{k_c,k_i-1}(\mathrm{j}\omega_{k_f}, \boldsymbol{\rho}))\operatorname{Im}(1 + L_{k_c,k_i}(\mathrm{j}\omega_{k_f}, \boldsymbol{\rho})) - \operatorname{Im}(1 + L_{k_c,k_i-1}(\mathrm{j}\omega_{k_f}, \boldsymbol{\rho}))\operatorname{Re}(1 + L_{k_c,k_i}(\mathrm{j}\omega_{k_f}, \boldsymbol{\rho}))}{\left|1 + L_{k_c,k_i-1}(\mathrm{j}\omega_{k_f}, \boldsymbol{\rho})\right|^2} \right) \pm \operatorname{atan2}\left(\frac{\operatorname{Im}(1 + G_{k_c}(\mathrm{j}\omega_{k_f}))}{\operatorname{Re}(1 + G_{k_c}(\mathrm{j}\omega_{k_f}))} \right) - \frac{\pi}{2} \leq 0$$
$$\text{when} \quad \pm \operatorname{Re}(1 + G_{k_c}(\mathrm{j}\omega_{k_f})) \geq 0 \tag{15e}$$

$$\pm \left(\operatorname{atan2}\left(\frac{\operatorname{Im}(1 + L_{k_c,k_i-1}(\mathrm{j}\omega_{k_f}, \boldsymbol{\rho}))}{\operatorname{Re}(1 + L_{k_c,k_i-1}(\mathrm{j}\omega_{k_f}, \boldsymbol{\rho}))} \right) + \frac{\operatorname{Re}(1 + L_{k_c,k_i-1}(\mathrm{j}\omega_{k_f}, \boldsymbol{\rho}))\operatorname{Im}(1 + L_{k_c,k_i}(\mathrm{j}\omega_{k_f}, \boldsymbol{\rho})) - \operatorname{Im}(1 + L_{k_c,k_i-1}(\mathrm{j}\omega_{k_f}, \boldsymbol{\rho}))\operatorname{Re}(1 + L_{k_c,k_i}(\mathrm{j}\omega_{k_f}, \boldsymbol{\rho}))}{\left|1 + L_{k_c,k_i-1}(\mathrm{j}\omega_{k_f}, \boldsymbol{\rho})\right|^2} \right) \mp \operatorname{atan2}\left(\frac{\operatorname{Im}(1 + G_{k_c}(\mathrm{j}\omega_{k_f}))}{\operatorname{Re}(1 + G_{k_c}(\mathrm{j}\omega_{k_f}))} \right) - \frac{\pi}{2} \leq 0$$
$$\text{when} \quad \pm \operatorname{Re}(1 + G_{k_c}(\mathrm{j}\omega_{k_f})) \geq 0 \tag{15f}$$

4. VERIFICATION OF DISTURBANCE REJECTION PERFORMANCE

In this section, the verification of disturbance rejection performance is conducted in a dual-stage actuator HDD benchmark problem. The result shows that the resonant filters are optimized with the conditions of robust stability, robust performance, and hardware constraints. The track-following performance with designed resonant filters outperforms that without resonant filters.

4.1 Conditions

The frequency response data is used from 100 Hz to Nyquist frequency $F_s/2 = 1/2T_s = 25.2\,\mathrm{kHz}$. The frequency response data is arranged at linearly even intervals in every 1 Hz and the number of data points is $n_f = 25101$. Nyquist diagram, sensitivity function, amplitude spectrum of e, and amplitude spectrum of y_p without resonant filters are shown in Fig. 7, Fig. 8, Fig. 9, and Fig. 10. From Fig. 9, the resonant filters are designed at eight frequencies with vertical black dotted lines, and the dumping coefficients of all resonant filters are set to $\zeta_r = 0.05$. For the initial condition, all tuning parameters are set to $\rho = 0$ and $F_{rp} = F_{rv} = 1$. In the robust stability condition, the modulus margin is set to $1/w_s = 6\,\mathrm{dB}$.

4.2 Optimization results

The optimization of the resonant filter design is conducted by YALMIP (Lofberg, 2004) and Mosek (Mosek, 2021) until the improvement of the objective function from the previous iteration becomes less than 0.1 %. Nyquist diagram, sensitivity function, amplitude spectrum of e, and amplitude spectrum of y_p with resonant filters are shown in Fig. 11, Fig. 12, Fig. 13, and Fig. 14. The optimization result shows that the resonant filters are designed with conditions of robust stability, robust performance, and hardware constraints in 9 cases of the controlled system.

4.3 Simulation results

The time domain simulation is conducted in a dual-stage actuator HDD benchmark problem without and with resonant filters in 9 cases of the controlled system. Fig. 15 shows the track-following performance. It shows that the tracking errors with resonant filters are smaller than those without resonant filters in all 9 cases. Fig. 16 shows the maximum stroke in a PZT actuator. It shows that the maximum stroke values with resonant filters are almost the same as those without resonant filters and both controlled systems satisfy the stroke limitation. As a result, the controlled system with resonant filters outperforms that without resonant filters.

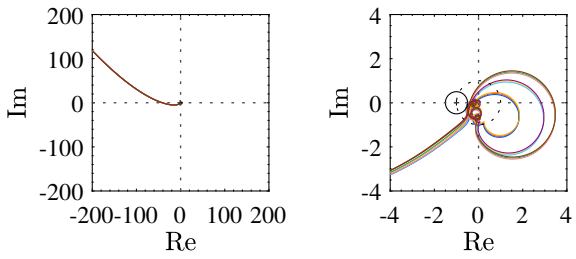

Fig. 7. Nyquist diagram without resonant filters.

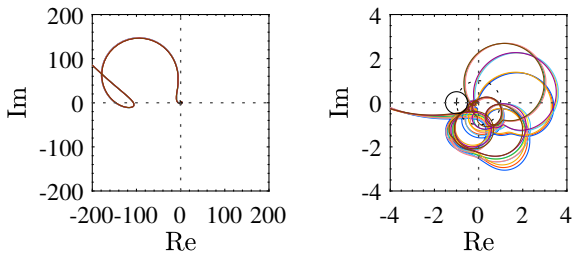

Fig. 11. Nyquist diagram with resonant filters.

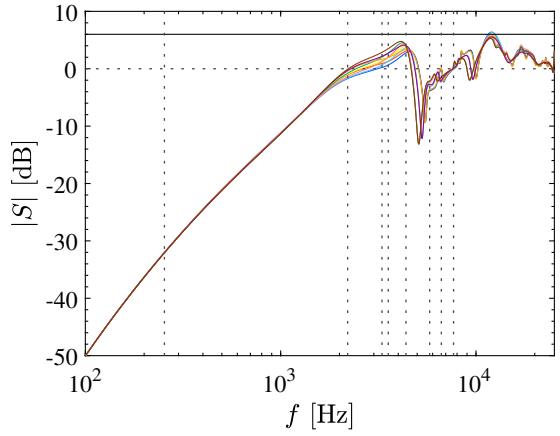

Fig. 8. Sensitivity function without resonant filters.

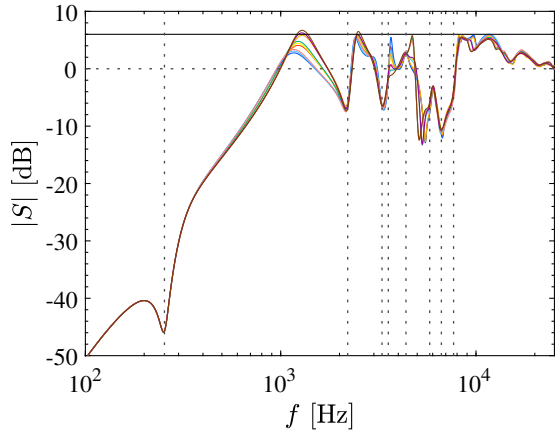

Fig. 12. Sensitivity function with resonant filters.

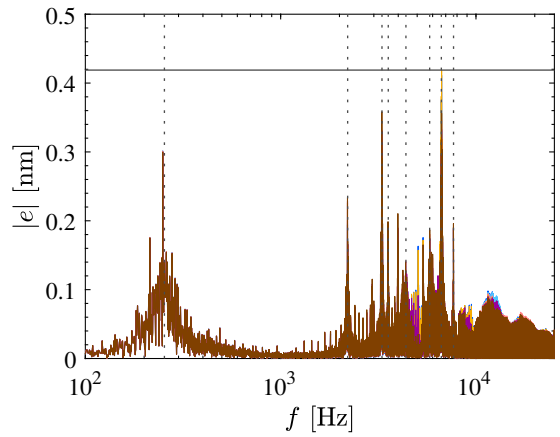

Fig. 9. Amplitude spectrum of e without resonant filters.

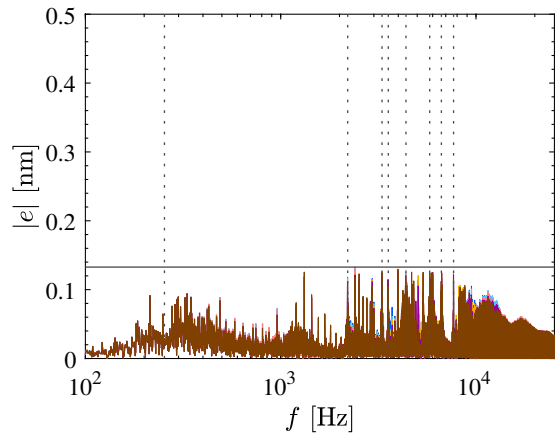

Fig. 13. Amplitude spectrum of e with resonant filters.

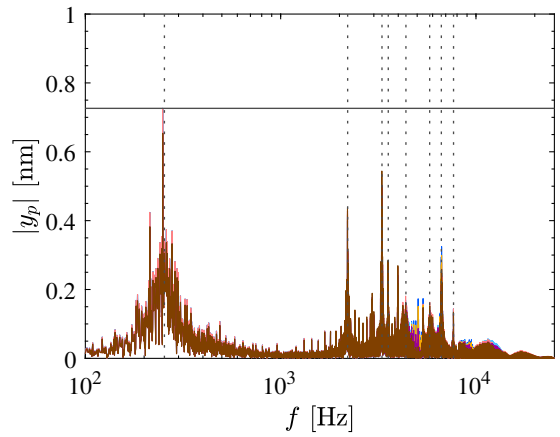

Fig. 10. Amplitude spectrum of y_p without resonant filters.

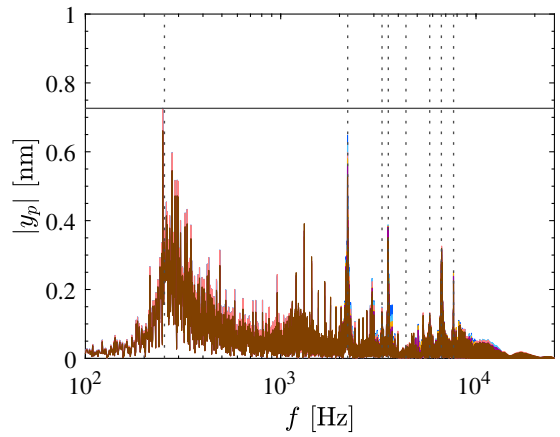

Fig. 14. Amplitude spectrum of y_p with resonant filters.

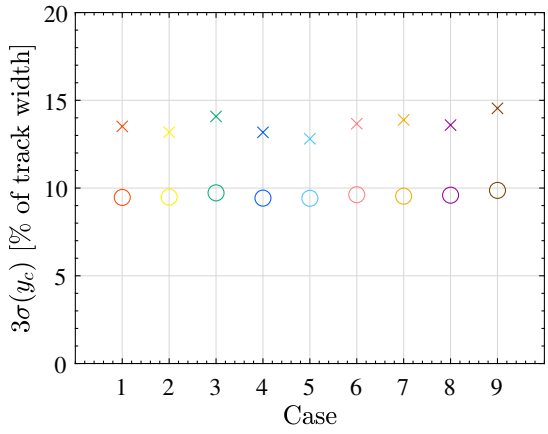

Fig. 15. Simulation results of track-following performance $3\sigma(y_c)$. × and ◯ denote without and with optimized resonant filters.

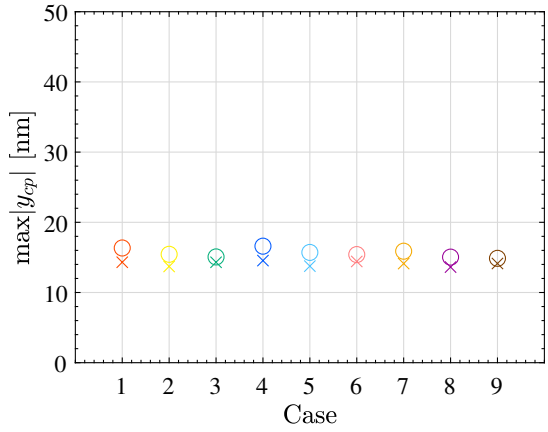

Fig. 16. Simulation results of maximum stroke in a PZT actuator max$|y_{cp}|$. × and ◯ denote without and with optimized resonant filters.

5. CONCLUSION

In this paper, the design method of optimal resonant filters is developed to improve track-following performance in a dual-stage actuator HDD. The resonant filters with structured parameterization are optimized by iterative convex optimization directly using the frequency response data of the controlled system. Robust stability, robust performance, and hardware constraints are considered for the optimization calculation in 9 cases of the controlled system. The disturbance rejection performance of the optimized resonant filters is validated in a dual-stage actuator HDD benchmark problem. Ongoing researches focus on the usage of both frequency domain and time domain data, designing other feedback controllers simultaneously, and the optimal design of multirate filters.

REFERENCES

Atsumi, T. (2016). Emerging Technology for Head-Positioning System in HDDs. *IEEJ Journal of Industry Applications*, 5(2), 117–122. doi:10.1541/ieejjia.5.117.

Atsumi, T. (2022). Magnetic-head positioning control system in HDDs. URL `https://jp.mathworks.com/matlabcentral/fileexchange/111515`.

Atsumi, T., Okuyama, A., and Kobayashi, M. (2007). Track-Following Control Using Resonant Filter in Hard Disk Drives. *IEEE/ASME Transactions on Mechatronics*, 12(4), 472–479. doi:10.1109/TMECH.2007.901944.

Bashash, S. and Shariat, S. (2019). Performance enhancement of hard disk drives through data-driven control design and population clustering. *Precision Engineering*, 56(November 2018), 267–279. doi:10.1016/j.precisioneng.2018.12.007.

Chen, X. and Tomizuka, M. (2014). New Repetitive Control With Improved Steady-State Performance and Accelerated Transient. *IEEE Transactions on Control Systems Technology*, 22(2), 664–675. doi:10.1109/TCST.2013.2253102.

Chen, X. and Tomizuka, M. (2016). Discrete-Time Reduced-Complexity Youla Parameterization for Dual-Input Single-Output Systems. *IEEE Transactions on Control Systems Technology*, 24(1), 302–309. doi:10.1109/TCST.2015.2422796.

Fujimoto, H. (2009). RRO Compensation of Hard Disk Drives With Multirate Repetitive Perfect Tracking Control. *IEEE Transactions on Industrial Electronics*, 56(10), 3825–3831. doi:10.1109/TIE.2009.2017558.

Lofberg, J. (2004). YALMIP : a toolbox for modeling and optimization in MATLAB. In *2004 IEEE International Conference on Robotics and Automation (IEEE Cat. No.04CH37508)*, 284–289. IEEE. doi:10.1109/CACSD.2004.1393890.

Mosek (2021). MOSEK 9.3. URL `https://www.mosek.com`.

Ohno, K. and Hara, T. (2006). Adaptive resonant mode compensation for hard disk drives. *IEEE Transactions on Industrial Electronics*, 53(2), 624–630. doi:10.1109/TIE.2006.870660.

Pérez-Arancibia, N.O., Tsao, T.C., and Gibson, J.S. (2010). A new method for synthesizing multiple-period adaptive–repetitive controllers and its application to the control of hard disk drives. *Automatica*, 46(7), 1186–1195. doi:10.1016/j.automatica.2010.04.007.

Potu Surya Prakash, N. and Horowitz, R. (2022). Data-Driven Robust Feedback Control Design for Multi-Actuator Hard Disk Drives. In *2nd IFAC Modeling, Estimation and Control Conference*.

Shahsavari, B., Keikha, E., Fu Zhang, and Horowitz, R. (2015). Adaptive Repetitive Control Design With Online Secondary Path Modeling and Application to Bit-Patterned Media Recording. *IEEE Transactions on Magnetics*, 51(4), 1–8. doi:10.1109/TMAG.2014.2364737.

Sun, L., Jiang, T., and Chen, X. (2017). Adaptive Loop Shaping for Wideband Disturbances Attenuation in Precision Information Storage Systems. *IEEE Transactions on Magnetics*, 53(5), 1–13. doi:10.1109/TMAG.2017.2654200.

Yabui, S., Atsumi, T., and Inoue, T. (2020). Coupling Controller Design for MISO System of Head Positioning Control Systems in HDDs. *IEEE Transactions on Magnetics*, 56(5), 1–9. doi:10.1109/TMAG.2020.2978156.

Zheng, M., Zhou, S., and Tomizuka, M. (2017). A design methodology for disturbance observer with application to precision motion control: An H-infinity based approach. In *2017 American Control Conference (ACC)*, 3524–3529. IEEE. doi:10.23919/ACC.2017.7963492.